

## UV-Photoelectron Spectroscopy of BN Indoles: Experimental and Computational Electronic Structure Analysis

Anna Chrostowska,<sup>\*,§</sup> Senmiao Xu,<sup>†,‡</sup> Audrey Mazière,<sup>§</sup> Katherine Boknevtz,<sup>†</sup> Bo Li,<sup>†</sup> Eric R. Abbey,<sup>‡,||</sup> Alain Dargelos,<sup>§</sup> Alain Graciaa,<sup>§</sup> and Shih-Yuan Liu<sup>\*,†,‡</sup>

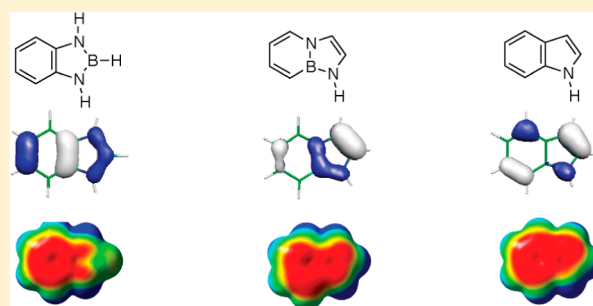
<sup>†</sup>Department of Chemistry, Boston College, Chestnut Hill, Massachusetts 02467, United States

<sup>‡</sup>Department of Chemistry, University of Oregon, Eugene, Oregon 97403-1253, United States

<sup>§</sup>Institut des Sciences Analytiques et de Physico-Chimie pour l'Environnement et les Matériaux, UMR CNRS 5254, Université de Pau et des Pays de l'Adour, Avenue de l'Université, 64 000 Pau, France

### Supporting Information

**ABSTRACT:** We present a comprehensive electronic structure analysis of two BN isosteres of indole using a combined UV-photoelectron spectroscopy (UV-PES)/computational chemistry approach. Gas-phase He I photoelectron spectra of external BN indole I and fused BN indole II have been recorded, assessed by density functional theory calculations, and compared with natural indole. The first ionization energies of these indoles are natural indole (7.9 eV), external BN indole I (7.9 eV), and fused BN indole II (8.05 eV). The computationally determined molecular dipole moments are in the order: natural indole (2.177 D) > fused BN indole II (1.512 D) > external BN indole I (0.543 D). The  $\lambda_{\max}$  in the UV-vis absorption spectra are in the order: fused BN indole II (292 nm) > external BN indole I (282 nm) > natural indole (270 nm). The observed relative electrophilic aromatic substitution reactivity of the investigated indoles with dimethyliminium chloride as the electrophile is as follows: fused BN indole II > natural indole > external BN indole I, and this trend correlates with the  $\pi$ -orbital coefficient at the 3-position. Nucleus-independent chemical shifts calculations show that the introduction of boron into an aromatic  $6\pi$ -electron system leads to a reduction in aromaticity, presumably due to a stronger bond localization. Trends and conclusions from BN isosteres of simple monocyclic aromatic systems such as benzene and toluene are not necessarily translated to the bicyclic indole core. Thus, electronic structure consequences resulting from BN/CC isosterism will need to be evaluated individually from system to system.



## 1. INTRODUCTION

Indole and its derivatives play pivotal roles in chemistry and biology. Important natural indoles include tryptamines melatonin<sup>1</sup> and serotonin,<sup>2</sup> which act as vital elements in brain function, as well as auxin, a crucial plant hormone,<sup>3</sup> which regulates gene expression associated with plant growth. 5,6-Dihydroxyindole serves as a universal precursor for natural pigments, and it is implicated in malignant melanoma.<sup>4</sup> Furthermore, natural indole alkaloids have been exploited for the treatment of a variety of human diseases. Currently in clinical use are anticancer agents vinblastine and vincristine, the antimigraine drug ergotamine, and the antiarrhythmic ajmalicine, to mention a few.<sup>5</sup> Because of the rich chemistry and biological activity of indole-containing natural products, chemists have been attracted to synthesis and study of non-natural indole derivatives. Indeed, synthetic variants of indole natural products have found wide-ranging applications as pharmaceuticals (e.g., iprindole, pindolol, and indomethacin).<sup>6</sup> A special natural indole derivative is the gene-encoded amino acid tryptophan.<sup>7</sup> It is the biological precursor to the majority of aforementioned indole natural products.<sup>5a</sup> Tryptophan occupies a unique

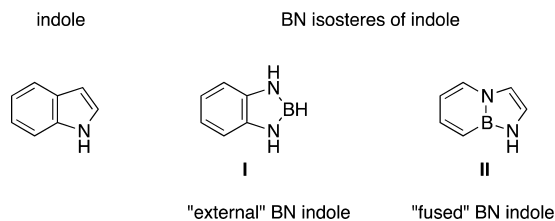
position among the canonical amino acids because of its ability to participate in a wide range of inter- and intramolecular interactions<sup>8</sup> and because it represents the main source of UV absorbance and fluorescence in proteins.<sup>9,10</sup> Tryptophan also plays a crucial role in enzymology. For instance, the tryptophan radical cation is actively involved in the reactivity of cytochrome c peroxidase, and it is implicated in long-range electron-transfer pathways in proteins (e.g., in DNA photolyases).<sup>11</sup>

Underlying the biochemistry and function of tryptophan and many indole-containing molecules is the 6,5 bicyclic indole motif (Scheme 1).<sup>12,13</sup> We have initiated a research program directed at expanding the chemical space of biologically active motifs through BN/CC isosterism,<sup>14</sup> i.e., the replacement of a carbon-carbon unit with the isosteric boron-nitrogen unit.<sup>15</sup> In view of the importance of the indole structure in biomedical research, we have directed our attention to apply the BN/CC isosterism to indole.<sup>16</sup> To date, two families of BN isosteres of indole have been developed, the “external” BN indoles (or

Received: June 25, 2014

Published: August 4, 2014

## Scheme 1. Indole and its BN Isosteres



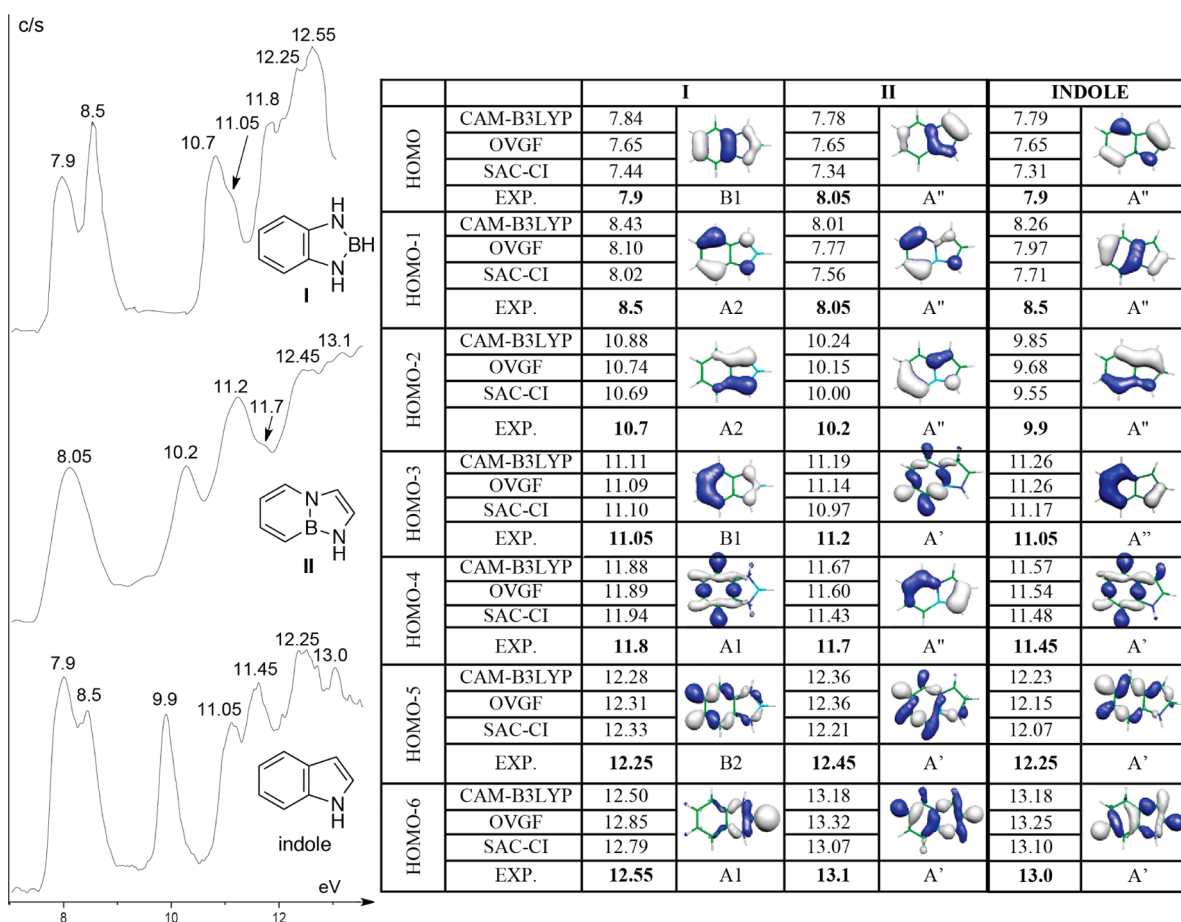
1,3,2-benzodiazaborolines) **I** and “fused” BN indoles **II** (Scheme 1). Goubeau reported the first example of an external BN indole in 1957 by treating trimethylboron with *o*-phenylenediamine.<sup>17</sup> He and his co-workers also prepared the parent external indole **I** in 1964.<sup>18</sup> Since Goubeau’s pioneering work, external BN indoles have been utilized as building blocks in optoelectronic materials<sup>19</sup> and as boryl ligands in organometallic chemistry.<sup>20</sup> The Liu group reported the first examples of fused BN indoles in 2010<sup>21</sup> and one year later disclosed the synthesis and characterization of the parent compound **II** (Scheme 1) of this family of indoles.<sup>22</sup> While the synthetic preparation of these compounds has been making steady progress, our understanding of the electronic structure of BN indoles (in particular that of fused BN indole) is still very limited. In this work, we provide a comprehensive electronic structure analysis of parental structures of BN indoles in direct

comparison to the natural indole using a combined UV-photoelectron spectroscopy (UV-PES)/computational chemistry approach.

UV-PES experimentally determines the gas-phase ionization energies (IEs) of molecules that can be correlated to the energies of occupied molecular orbitals. For a reliable assignment of UV photoelectron spectroscopic bands and for the interpretation of spectra, a combined UV-PES/theoretical approach is necessary. The Chrostowska group has calibrated different computational methods (e.g., the standard outer valence green function (OVGF), density functional theory (DFT), self-consistent field/time-dependent density functional theory ( $\Delta$ SCF/TD-DFT), TD-DFT, complete active space second-order perturbation theory (CASPT2), and statistical average of different orbital model potential exchange–correlation functional (SAOP XC) against the experimentally determined UV-PES IEs.<sup>23</sup> The combined UV-PES/computational modeling approach developed by Chrostowska and co-workers is used to investigate the electronic structure of the compounds illustrated in Scheme 1.

## 2. EXPERIMENTAL AND COMPUTATIONAL METHODS

**Coupled UV-PES–Mass Spectrometry Measurements.** The UV-PES spectra were recorded on a home-built (IPREM/ECP), three-part spectrometer equipped with a main body device, He–I radiation source (21.21 and/or 48 eV), and a 127° cylindrical analyzer. The



**Figure 1.** UV-PES spectra of external BN indole **I**, fused BN indole **II**, and natural indole. The seven HOMOs with the corresponding IEs for each of the three molecules are illustrated. The table shows the calculated Kohn–Sham MO shapes and symmetries (MOLEKEL visualization) and calculated  $\Delta$ SCF/TD-DFT (CAM-B3LYP), OVGF, and SAC–CI IEs of natural indole, **I**, and **II**, in comparison with experimental IE values (in eV). For all calculations 6-311G(d,p) basis set was applied; iso value =  $\pm 0.05$  e/bohr<sup>-3</sup>.

spectrometer works at constant analyzer energy under  $5 \times 10^{-6}$  hPa working pressure and  $\leq 10^{-7}$  hPa for channeltron (X914L) pressure. The monitoring is done by a microcomputer supplemented by a digital–analogue converter (AEI spectrum). The spectra resulting from a single scan are built from 2048 points and are accurate within 0.05 eV. Spectra are calibrated with lines of xenon (12.13 and 13.44 eV) and of argon (15.76 and 15.94 eV). The accuracy of the IEs is  $\pm 0.03$  eV for sharp peaks and  $\pm 0.05$  eV for broad and overlapping signals. Mass spectra were recorded on a modified quadrupole mass spectrometer (PFEIFFER Prisma QMS200) with an electron-impact at 50 eV (mass range: 200 amu; detection limit:  $\leq 10^{-14}$  hPa; working pressure:  $2 \times 10^{-9}$  hPa; operating temperature: 200 °C; electronic amplifier in working conditions:  $10^{-10}$  A, QUAD STAR422 software for recording and treatment of MS data). The samples were slowly vaporized under low pressure ( $10^{-6}$  Torr) inside a handmade three-valve injector (3/4 in. diameter; 10 cm length; working temperature:  $-190 \leq T \leq +300$  °C), and the gaseous flow was then continuously and simultaneously analyzed by both UV-photoelectron and mass spectrometers.

**Computational Methods.** All calculations were performed using the Gaussian 09<sup>24</sup> program package with the 6-311G(d,p)<sup>25</sup> basis set. Extra diffuse functions (6-311++G(d,p)) are included in the basis set to improve the description of the electron affinities (EA). DFT has been shown to predict various molecular properties of similar compounds successfully.<sup>26</sup> All geometry optimizations were carried out with the CAM-B3LYP<sup>27</sup> functionals and were followed by frequency calculations in order to verify that the stationary points obtained were true energy minima. Ionization energies were calculated with  $\Delta$ SCF-DFT, which means that separate SCF calculations were performed to optimize the orbitals of the ground state and the appropriate ionic state ( $IE = E_{\text{cation}} - E_{\text{neutral}}$ ). The advantages of the most frequently employed  $\Delta$ SCF-DFT method of calculations of the first IEs have been demonstrated previously.<sup>28</sup> The TD-DFT<sup>23,29</sup> approach provides a first-principal method for the calculation of excitation energies within a density functional context taking into account the low-lying ion calculated by the  $\Delta$ SCF method (the excitation energies of the radical cation obtained from a TD-DFT treatment were added to the IE that was computed with the  $\Delta$ SCF-DFT method). The vertical IEs were also calculated at the ab initio level according to OVG<sup>30</sup> (in this case the effects of electron correlation and reorganization are included beyond the Hartree–Fock approximation and the self-energy part was expanded up to third order) and SAC–CI<sup>31</sup> (symmetry adapted cluster/configuration interaction methods of Nakatsuji and co-workers which describes accurately and efficiently the electronic structures of the excited, ionized and electron-attached states of molecules) methods. MOLEKEL<sup>32</sup> was used as a visualization tool for all MOs.

### 3. RESULTS AND DISCUSSION

**UV-PES Analysis.** The UV-photoelectron spectra of external BN indole **I** and fused BN indole **II** are illustrated in Figure 1. The known UV-PE spectrum of indole<sup>33</sup> is also given to allow a direct comparison with the compounds under current investigation.<sup>34</sup> For the reliable assignment of PE bands, DFT ( $\Delta$ SCF/TD-DFT (CAM-B3LYP)) and ab initio (OVGF and SAC–CI) calculations of IEs using the 6-311G(d,p) basis set have been carried out on optimized geometrical parameters of BN indoles **I** and **II**. The comparison of the theoretically predicted IEs and experimental observed data is summarized in the Table in Figure 1. It appears that the DFT calculations (CAM-B3LYP) best model the experimentally determined IEs.

Indole belongs to the  $C_s$  point group. The photoelectron spectrum of natural indole exhibits a low-energy band at 7.9 eV which is associated with its HOMO of  $\pi$  symmetry ( $A''$ ). The second (HOMO-1), third (HOMO-2), and fourth (HOMO-3) bands correspond also to MO of  $\pi$  symmetry ( $A''$ ) and are located at 8.5, 9.9, and 11.05 eV, respectively. Similar to indole,

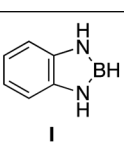
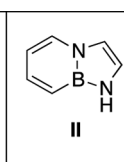
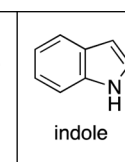
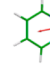
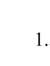
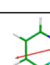
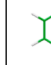
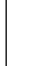

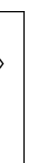


the fused BN indole **II** has also  $C_s$  symmetry. The first broad PE band located at 8.05 eV contains two  $A''$ -symmetry MO (HOMO and HOMO-1) ionizations. The next ionization at 10.2 eV is also linked with a MO (HOMO-2) of  $A''$  symmetry, while the fourth ionization at 11.2 eV corresponds to a MO (HOMO-3) of  $\sigma$  symmetry ( $A'$ ). In contrast to natural indole and fused BN indole, the external BN indole **I** has  $C_{2v}$  symmetry. The first PE band for BN indole **I** appears at the same IE value as for indole molecule (at 7.9 eV) and corresponds to the antibonding combination of the delocalized NBN  $\pi$  system with benzene  $\pi$  system ( $B_1$  symmetry ( $\pi_1 - \pi_{\text{NBN}}$ )). The second sharp and intense band located at 8.5 eV (HOMO-1) is attributed to a MO with  $A_2$  symmetry featuring two nitrogen lone pairs and  $\pi$ -antibonding interactions in the benzene ring ( $n_{\text{N}} - \pi_{\text{C}=\text{C}}$ ). The third PE band (HOMO-2) at 10.7 eV and a shoulder at 11.05 eV (HOMO-3) reflect the ionizations from orbitals of  $A_2$  ( $\pi_{\text{CCN}}$ ) and  $B_1$  ( $\pi_2 - \pi_{\text{NBN}}$ ) symmetry, respectively. The higher-energy bands (>12.2 eV) for all three molecules are associated with MOs of various  $\sigma$  symmetries ( $A'$ ,  $A_1$ ,  $B_2$ ). It should be noted that the chosen computational models agree reasonably well with the experimentally determined IEs.

The comparison of these experimental and computational data (Figure 1) shows that the replacement of two adjacent carbon atoms in indole by nitrogen and boron does not result in significant changes in the energy level of the corresponding HOMOs, a finding which is in stark contrast to simple monocyclic arenes<sup>35,36</sup> where BN/CC isosterism leads to significant destabilization of the HOMO.<sup>37</sup> The molecular structure change associated with the external BN indole **I** relative to natural indole does not cause any changes in the energy level for the HOMO-1; both MOs have IEs at 8.5 eV. On the other hand, the HOMO-1 for the fused BN indole **II** is destabilized by 0.45 eV relative to the corresponding MO for the natural indole. For HOMO-2, the following energetic trend is observed: external BN indole **I** at 10.7 eV IE is most stable followed by fused BN indole **II** at 10.2 eV IE and natural indole at 9.9 eV IE. The IEs for HOMO-3 for all three indole molecules are fairly similar ( $\sim 11.1$  eV). However, while HOMO-3 in fused BN indole **II** has  $\sigma$  symmetry ( $A'$ ), the HOMO-3 for natural indole and the external BN indole **I** have  $\pi$  symmetry ( $A''$  and  $B_1$ , respectively).

According to the frontier molecular orbital theory,<sup>38</sup> the electronic structure determination of the HOMO is the most significant in terms of property and reactivity predictions. Despite the similar HOMO energy levels of natural indole and BN indoles **I** and **II**, the nature of these HOMOs is quite distinct. The HOMO of the indole system can be best described as the antibonding combination of the nitrogen lone pair (in indole) or the NBN  $\pi$  system (in compounds **I** and **II**) with an adjacent carbon  $\pi$  system. Because of the different locations of the BN unit in **I** and **II** and thus different symmetries, the orbital coefficient distributions are quite different between **I** and **II**, a result that may shed some light into the different properties and reactivities between the BN indole families (*vide infra*). The natural indole and fused BN indole share the same symmetry point group ( $C_s$ ). Thus, it appears from Figure 1 that the electronic structure of natural indole more resembles that of fused BN indole **II** than that of external BN indole **I**, and one might predict similar reactivity patterns between natural indole and BN indole **II** as a consequence (*vide infra*).

**Additional Computational Results.** We have investigated the ground-state dipole moments of the three indole compounds. As can be seen from Table 1, CAM-B3LYP/6-

**Table 1. CAM-B3LYP/6-311G(d,p) Ground and First Excited-State Dipole Moment (Debye), Electrostatic Potential Map at the 0.001 Electron au Density Isocontour Level (from +12.55 to -12.55 kcal/mol),  $\Delta$ SCF IE (eV), Kohn–Sham Energies (eV) of HOMO, LUMO, and HOMO–LUMO Gap (eV)<sup>a</sup>**

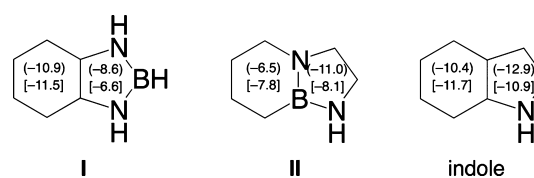
			
ground state dipole moment [Debye]	 0.543	 1.512	 2.177
first excited state dipole moment [Debye]	 1.102	 4.080	 2.471
electrostatic potential surface map			
HOMO [eV]	-7.14	-7.06	-7.05
LUMO [eV]	1.15	0.74	0.89
HOMO-LUMO gap [eV]	8.29	7.80	7.94
$\Delta$ SCF/TD-DFT ionization energy (IE) [eV]	7.84	7.78	7.79
electron affinity (EA) [eV]	-1.24	-1.01	-0.56
$\Delta$ (IE+EA) [eV]	6.60	6.77	7.23
First HOMO $\rightarrow$ LUMO transition [eV]	5.02	4.84	5.05

<sup>a</sup>CAM-B3LYP/6-311++G(d,p) electron affinity (eV),  $\Delta$ (IE-EA) and first HOMO  $\rightarrow$  LUMO UV transition (eV) for BN indoles I, II, and natural indole.

311G(d,p) calculations predict the following trend in molecular dipole moments in the order of increasing strength: BN indole I (0.543 D), BN indole II (1.512 D), and natural indole (2.177 D). It is worth noting that while BN isosteres of monocyclic arenes are significantly more polar (by >1.5 D) than their carbonaceous counterparts,<sup>35</sup> the BN indoles in this study exhibit weaker dipole moments than the natural indole. TD-DFT calculations suggest that the direction of the dipole moments does not significantly change upon excitation of the ground state to the first excited state for all three indoles. On the other hand, the magnitude of the dipole moment can

change dramatically depending on the structure. An increase in polarity by 0.29 and 0.56 D is predicted for natural indole and BN indole I upon excitation to the first excited state, respectively. Uniquely, a polarity increase of 2.57 D is predicted for the fused BN indole II upon excitation to the first excited state. The direction and magnitude of the ground-state dipole moments are consistent with the calculated electrostatic potential surface (EPS) maps for the three indoles at the 0.001 electron au density isocontour level. The color red indicates negative charge, whereas the color blue represents positive charge. Qualitatively, the EPS maps illustrate that the “higher” symmetry of BN indoles I and II (i.e., two electronegative N atoms are arranged in relatively symmetrical fashion) minimizes the overall dipole moment compared to natural indole. For the external BN indole I, the negative charge is mostly localized on the six-membered carbocyclic ring while the positive charge is located at the N-substituent. The boron atom in the external BN indole I is also devoid of negative charge, consistent with the relatively electropositive character of boron. In contrast to the external BN indole I, significant negative charge can be found near the boron position in the fused BN indole II, and the liver-shaped negative charge distribution in BN indole II resembles that of natural indole. The observation of significant negative charge at the least electronegative boron atom in fused BN indole II is consistent with strong resonance/ $\pi$  electron delocalization effects that provide the boron atom with extra negative charge.<sup>39</sup> Conversely, the lack of negative charge at the boron position in the external BN indole I suggests that the electron density is less delocalized in the five-membered ring system of I relative to II and indole. Noteworthy is the trend for predicted electron affinities. The comparison of calculated electron affinities (CAM-B3LYP/6-311++G(d,p)) for the three indole molecules indicates that external BN indole I exhibits the most negative electron affinity, followed by fused BN indole II and natural indole.

Figure 2 shows the calculated nucleus-independent chemical shifts (NICS) (0) (in parentheses) and NICS (1) [in brackets]

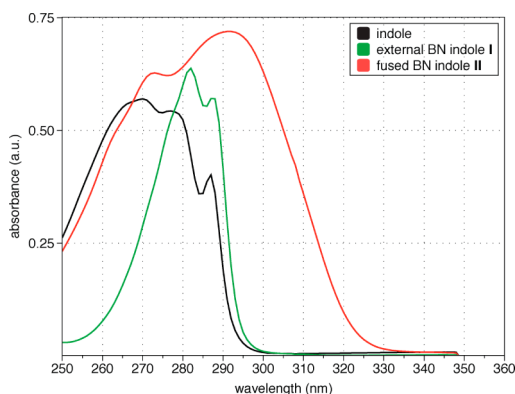


**Figure 2.** Calculated (CAM-B3LYP/6-311(d,p)) NICS (0) (in parentheses) and NICS (1) [in brackets] values of BN indoles I, II and natural indole.

values<sup>40</sup> of the five- and six-membered rings of BN indoles I and II and indole. Indole is an aromatic heterocycle as evidenced by the strongly negative NICS values for both the five- and six-membered rings. The replacement of CC with BN at the 8,9-positions in fused BN indole II introduces localization of electron density and reduces the aromatic ring current as evidenced by the less negative NICS values. Interestingly, a stronger reduction of aromaticity is observed for the six-membered ring vs the five-membered ring. For the external BN indole I, the aromatic character of the six-membered carbocyclic ring is retained. However, strong localization of electron density is observed for the five-membered heterocyclic ring as evidenced by the relatively less negative NICS values. This observation is also consistent

with the EPS map for compound I, in which a stronger electron localization is predicted.

**Correlation of Experimental Characterization with UV-PES/Computational Electronic Structure Data. UV-vis Absorption Spectra.** Figure 3 displays the experimental



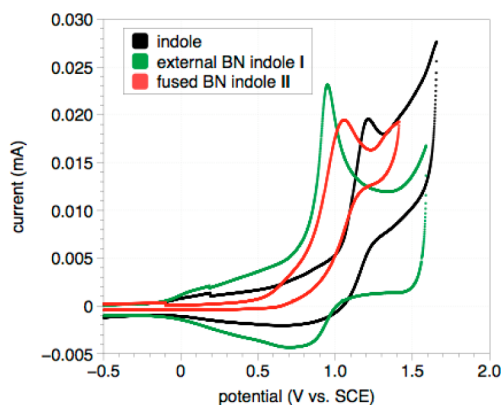
entry	compound	$\lambda_{\text{max}}(\text{calc})$ (nm)	$\lambda_{\text{max}}(\text{exp})^{\text{a}}$ (nm)	oscillator strength (calc)
1	indole	243	270	0.109
2	BN indole I	247	282	0.111
3	BN indole II	256	292	0.160

<sup>a</sup> measured in MeCN at  $10^{-4}$  M concentration.

**Figure 3.** Comparison of TD-DFT calculations (CAM-B3LYP/6-311++G(d,p)) and observed UV-vis absorption spectra for indole and BN indoles I and II.

UV-vis absorption spectra<sup>41</sup> and the calculated absorption maxima of indole and BN indoles I and II. The highest probability low-energy transition for natural indole is calculated to be at 243 nm. This band is observed in the UV-vis spectrum at  $\lambda_{\text{max}} = 270$  nm (Figure 3, entry 1). In the case of external BN indole I, the  $\lambda_{\text{max}}$  is calculated to be at 247 nm and is experimentally observed at  $\lambda_{\text{max}} = 282$  nm (Figure 3, entry 2). For fused BN indole II, the lowest-energy absorption band is calculated to be at 256 nm and is observed at  $\lambda_{\text{max}} = 292$  nm (Figure 3, entry 3). In comparison to the theoretically derived gas-phase values, the experimentally observed  $\lambda_{\text{max}}$  values are bathochromically shifted by  $\sim 4500$   $\text{cm}^{-1}$ . A similar difference is also observed for monocyclic arenes.<sup>35</sup>

**Electrochemistry.** As established by previous UV-PES experiments, BN/CC isosterism of simple monocyclic arenes (e.g., benzene and toluene) leads to heterocycles with higher HOMO energy levels ( $>0.38$  eV).<sup>35</sup> On the other hand, the HOMOs of BN indoles I and II in this study do not appear to have higher energy levels than the natural indole. In fact, the HOMO of fused BN indole II is somewhat stabilized relative to natural indole according to the experimental gas-phase UV-PES analysis (Figure 1). Cyclic voltammetry also probes the HOMO energy levels of molecules, albeit in the solution phase, where dipole moment and solvent polarity may additionally influence the oxidation potential. Figure 4 illustrates that all oxidations are irreversible and centered around 1.0 V potential vs saturated calomel electrode (SCE).<sup>42</sup> Natural indole has an oxidation wave peaking at 1.22 V vs SCE, compared to 1.05 and 0.95 V measured for BN indole II and BN indole I vs SCE in MeCN, respectively. The difference in oxidation potential of  $\sim 0.3$  V between natural indole and its BN isosteres I and II is significantly smaller than the observed difference of  $\sim 1$  V in oxidation potentials between benzene and 1,2-dihydro-1,2-

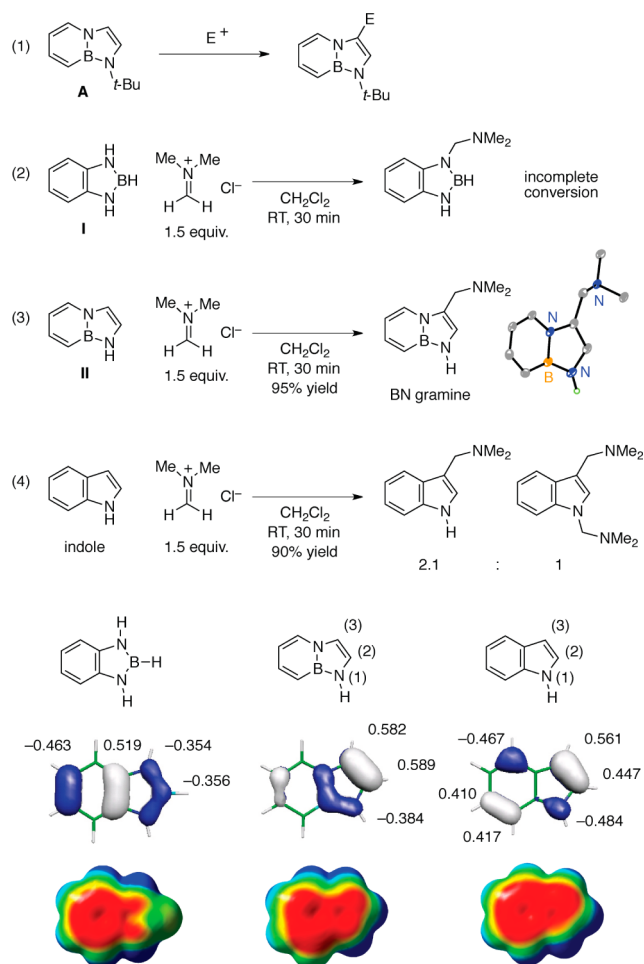


**Figure 4.** Cyclic voltammograms of indole, BN indole I, and BN indole II (0.1 M TBAPF<sub>6</sub> in MeCN; scan rate, 50 mV/s).

azaborine.<sup>35</sup> It is also worth noting that the anodic peak potential trend correlates with calculated dipole moment of the indoles. It appears that the relatively polar acetonitrile solvent is exerting some stabilizing effect on indoles with stronger ground-state dipole moments.<sup>43</sup>

**Chemical Reactivity.** We have previously determined that the *N*-*t*-Bu-substituted fused BN indole A undergoes electrophilic aromatic substitution (EAS) reactions with the same regiochemistry as natural indole, i.e., preferentially at the three-position (Figure 5, eq 1).<sup>21</sup> In this study, we investigated the EAS behavior of the parental structures. To the best of our knowledge, EAS reactions of external BN indole I has not been reported. Treatment of BN indole I with dimethyliminium chloride showed incomplete conversion (ratio of starting material to product  $\sim 1.3:1$ , see Supporting Information for details) at room temperature with 30 min reaction time (Figure 5, eq 2).<sup>44</sup> On the other hand, the fused BN indole II reacted cleanly with the dimethyliminium electrophile to furnish the C3-substituted product in 95% yield and complete regioselectivity under identical conditions as in eq 2 (Figure 5, eq 3). We were able to obtain the X-ray crystal structure of the EAS product and thus unambiguously determine the substitution pattern. It is worth noting that the product illustrated in eq 3 is a BN isostere of the biologically active indole alkaloid gramine.<sup>45</sup> In a direct comparison, natural indole reacts with dimethyliminium chloride<sup>46</sup> to give a mixture of two products, gramine and its bisalkylated adduct, in approximately 2.1 to 1 ratio, respectively (Figure 5, eq 4).<sup>47</sup>

The regioselective EAS reaction of the parent fused BN indole II is somewhat surprising if one considers only the HOMO  $\pi$ -orbital coefficients, which are very similar for the 2- and 3-carbon positions (0.589 vs 0.582). However, the EPS map of BN indole II indicates an apparent localization of negative charge around the 3-position.<sup>48</sup> Thus, the observed EAS regioselectivity for BN indole II could potentially be rationalized by the synergistic combination of both the frontier orbital coefficients and the charge distribution. Similar to BN fused indole II, the regioselectivity for natural indole is consistent with the  $\pi$ -orbital coefficient distribution in the HOMO and the charge distribution according to the EPS map (Figure 5, bottom right). Despite the relatively low oxidation potential (see Figure 4) the external indole does not undergo substitution reactivity with dimethyliminium chloride efficiently at the corresponding “3”-position (i.e., at nitrogen). This is consistent with the relatively small HOMO  $\pi$ -orbital coefficient at nitrogen for compound I (Figure 5, bottom left).<sup>49,50</sup> It



**Figure 5.** HOMO with corresponding  $\pi$ -orbital coefficients, and electrostatic potential surface at the 0.001 electron au density isocontour level (+12.55 to  $-12.55$  kcal mol $^{-1}$ ) of external BN indole I (left), fused BN indole II (middle), and natural indole (right). Red indicates negative charge, and blue indicates positive charge.

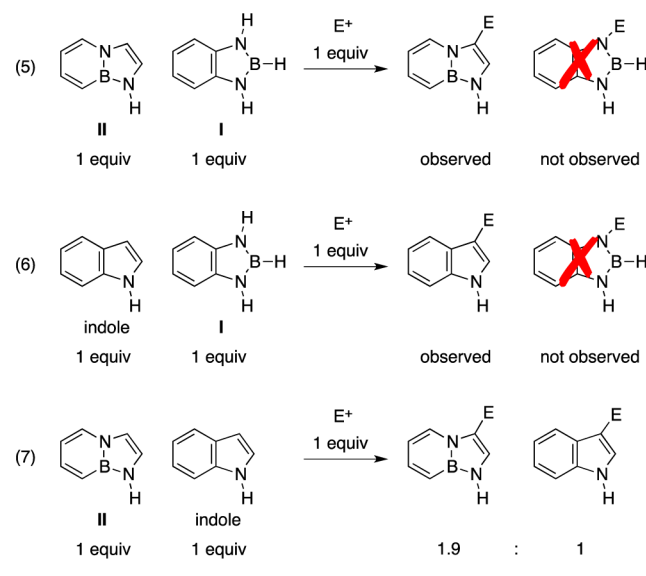
appears that the HOMO  $\pi$ -orbital coefficient and the charge distribution are the dominant factors in determining relative reactivity and selectivity rather than the HOMO energy levels.

We have also performed direct EAS competition experiments<sup>21</sup> among the parental indole structures. Using 1 equiv of each BN indole II, BN indole I, and dimethyliminium chloride in  $\text{CD}_2\text{Cl}_2$ , we observed exclusively the EAS adduct associated with fused BN indole II (Scheme 2, eq 5). Similarly, a competition experiment between natural indole and external BN indole I showed exclusive formation of the EAS adduct of natural indole (Scheme 2, eq 6). Finally, a competition experiment between fused BN indole II and natural indole revealed a preference for the electrophile to react with the fused BN indole II (Scheme 2, eq 7). Thus, the relative EAS reactivity for the parental indoles is as follows: fused BN indole II > natural indole > external BN indole I. This trend correlates with the  $\pi$ -orbital coefficient at the 3-position which are 0.582, 0.561, and 0.354 for BN indole II, indole, and BN indole I, respectively.

#### 4. CONCLUSION

In summary, we described a comprehensive electronic structure analysis of BN indoles I and II in direct comparison with the natural indole using a combined UV-PES/computational

#### Scheme 2. EAS Competition Experiments with Dimethyliminium Chloride as the Electrophile



chemistry approach. In contrast to monocyclic arenes, BN/CC isosterism in the context of indole does not result in significant changes in the energy level of the HOMOs. Gas-phase UV-PES studies revealed the following HOMO energies: natural indole ( $-7.9$  eV), external BN indole I ( $-7.9$  eV), and fused BN indole II ( $-8.05$  eV). Furthermore, while BN isosteres of benzene and toluene exhibit stronger ground-state dipole moments than their carbonaceous counterparts, external BN indole I (0.543 D) and fused BN indole II (1.512 D) are significantly less polar than the natural indole (2.177 D). On the other hand, the lower band gap observed for BN isosteres of benzene and toluene vs their carbonaceous counterparts is also observed for the indole system. The trend for  $\lambda_{\text{max}}$  in the UV-vis absorption spectrum (longest to shortest wavelength) is as follows: fused BN indole II (292 nm) > external BN indole I (282 nm) > natural indole (270 nm). While the experimental gas-phase UV-PES data of the indole molecules do not show a particular trend with regard to the first IE, electrochemistry data in solution phase reveal a small trend with regard to the anodic peak potential (lowest to highest): external BN indole I (0.95 V) < fused BN indole II (1.05 V) < natural indole (1.22 V). The observed relative electrophilic aromatic substitution reactivity of the investigated indoles is as follows: fused BN indole II > natural indole > external BN indole I. This trend correlates with the  $\pi$ -orbital coefficient at the 3-position. NICS calculations show that the introduction of boron into an aromatic  $6\pi$ -electron system leads to a reduction in aromaticity, presumably due to a stronger bond localization. We conclude from this study that trends and conclusions from BN isosteres of simple monocyclic aromatic systems such as benzene and toluene are not necessarily translated to the bicyclic indole core. Electronic structure consequences resulting from BN/CC isosterism will need to be evaluated individually from system to system.

#### ■ ASSOCIATED CONTENT

##### Supporting Information

Experimental procedures, spectroscopic data, complete ref 24, and additional computational data. This material is available free of charge via the Internet at <http://pubs.acs.org>.

## ■ AUTHOR INFORMATION

## Corresponding Authors

shihyuan.liu@bc.edu  
anna.chrostowska@univ-pau.fr

## Present Address

<sup>||</sup>Department of Chemistry and Biochemistry, Eastern Washington University, Cheney, WA 99004

## Notes

The authors declare no competing financial interest.

## ■ ACKNOWLEDGMENTS

Support has been provided by the National Institutes of Health (National Institute of General Medical Sciences, Grant R01-GM094541). A.C. and A.M. are grateful to the Communauté de Communes de Lacq (France) for financial support.

## ■ REFERENCES

- (1) For a leading reference, see: Arendt, J. *J. Biol. Rhythms* **2005**, *20*, 291–303.
- (2) For a review of serotonin, see: Gingrich, J. A.; Hen, R. *Psychopharmacology* **2001**, *155*, 1–10.
- (3) For leading references, see: (a) Everts, S. *Chem. Eng. News* **2007**, *85* (15), 11. (b) Tan, X.; Calderon-Villalobos, L. I. A.; Sharon, M.; Zheng, C.; Robinson, C. V.; Estelle, M.; Zheng, N. *Nature* **2007**, *446*, 640–645.
- (4) Tsukamoto, K.; Palumbo, A.; D'Ischia, M.; Hearing, V. J.; Prota, G. *Biochem. J.* **1992**, *286*, 491–495.
- (5) For reviews on indole alkaloid natural products, see: (a) O'Connor, S. E.; Maresh, J. *J. Nat. Prod. Rep.* **2006**, *23*, 532–547. (b) Gul, W.; Hamann, M. T. *Life Sci.* **2005**, *78*, 442–453.
- (6) For a review, see: Gupta, R. R.; Kumar, M.; Gupta, V. *Heterocyclic Chemistry II*; Springer: Berlin, 1998; Vol. 2, Chapter 3.
- (7) For leading references, see: (a) Bao, Z.; Sun, S.; Li, J.; Chen, X.; Dong, S.; Ma, H. *Angew. Chem., Int. Ed. Engl.* **2006**, *45*, 6723–6725. (b) Budisa, N.; Rubini, M.; Bae, J. H.; Weyher, E.; Wenger, W.; Golbik, R.; Huber, R.; Moroder, L. *Angew. Chem., Int. Ed. Engl.* **2002**, *41*, 4066–4069.
- (8) (a) Dougherty, D. A. *J. Nutr.* **2007**, *137*, 1504S–1508S. (b) Dougherty, D. A. *J. Org. Chem.* **2008**, *73*, 3667–3673. (c) Burley, S. K.; Petsko, G. A. *Science* **1985**, *229*, 23–28.
- (9) Callis, P. R. *Methods Enzymol.* **1997**, *278*, 113–150.
- (10) Lippitz, M.; Erker, W.; Decker, H.; van Holde, K. E.; Basché, T. *Proc. Natl. Acad. Sci. U. S. A.* **2002**, *99*, 2772–2777.
- (11) For a review of protein radicals, see: Stubbe, J.; van der Donk, W. A. *Chem. Rev.* **1998**, *98*, 705–762.
- (12) Baeyer, A.; Emmerling, A. *Ber. Dtsch. Chem. Ges.* **1869**, *2*, 679–682.
- (13) For an overview of indole synthesis, see: Taber, D. F.; Tirunahari, P. K. *Tetrahedron* **2011**, *67*, 7195–7210.
- (14) For leading references on BN isosteres in the biomedical context, see: (a) Zhou, H. B.; Nettles, K. W.; Bruning, J. B.; Kim, Y.; Joachimiak, A.; Sharma, S.; Carlson, K. E.; Stossi, F.; Katzenellenbogen, B. S.; Greene, G. L.; Katzenellenbogen, J. A. *Chem. Biol.* **2007**, *14*, 659–669. (b) Ito, H.; Yumura, K.; Saigo, K. *Org. Lett.* **2010**, *12*, 3386–3389. (c) Liu, L.; Marwitz, A. J.; Matthews, B. W.; Liu, S.-Y. *Angew. Chem., Int. Ed. Engl.* **2009**, *48*, 6817–6819. (d) Knack, D. H.; Marshall, J. L.; Harlow, G. P.; Dudzik, A.; Szaleniec, M.; Liu, S.-Y.; Heider, J. *Angew. Chem., Int. Ed. Engl.* **2013**, *52*, 2599–2601.
- (15) For an overview, see: (a) Liu, Z.; Marder, T. B. *Angew. Chem., Int. Ed. Engl.* **2008**, *47*, 242–244. (b) Bosdet, M. J. D.; Piers, W. E. *Can. J. Chem.* **2009**, *87*, 8–29. (c) Campbell, P. G.; Marwitz, A. J.; Liu, S.-Y. *Angew. Chem., Int. Ed. Engl.* **2012**, *51*, 6074–6092.
- (16) Abbey, E. R.; Liu, S.-Y. *Org. Biomol. Chem.* **2013**, *11*, 2060–2069.
- (17) Ulmschneider, D.; Goubeau, J. *Chem. Ber.* **1957**, *90*, 2733–2738.
- (18) Goubeau, J.; Schneider, H. *Liebigs. Ann. Chem.* **1964**, *675*, 1–9.
- (19) For leading references, see: (a) Weber, L.; Werner, V.; Fox, M. A.; Marder, T. B.; Scwedler, S.; Brockhinke, A.; Stammler, H. G.; Neumann, B. *Dalton Trans.* **2009**, 1339–1351. (b) Weber, L.; Werner, V.; Fox, M. A.; Marder, T. B.; Scwedler, S.; Brockhinke, A.; Stammler, H.-G.; Neumann, B. *Dalton Trans.* **2009**, 2823–2831. (c) Chrostowska, A.; Maciejczyk, M.; Dargelos, A.; Baylère, P.; Weber, L.; Werner, V.; Eickhoff, D.; Stammler, H. G.; Neumann, B. *Organometallics* **2010**, *29*, 5192–5198. (d) Maruyama, S.; Kawanishi, Y. *J. Mater. Chem.* **2002**, *12*, 2245–2249. (e) Kubo, Y.; Tsuruzoe, K.; Okuyama, S.; Nishiyabu, R.; Fujihara, T. *Chem. Commun.* **2010**, 46, 3604–3606.
- (20) For leading references, see: (a) Habereeder, T.; Nöth, H. *Appl. Organomet. Chem.* **2003**, *17*, 525–538. (b) Segawa, Y.; Suzuki, Y.; Yamashita, M.; Nozaki, K. *J. Am. Chem. Soc.* **2008**, *130*, 16069–16079. (c) Segawa, Y.; Yamashita, M.; Nozaki, K. *J. Am. Chem. Soc.* **2009**, *131*, 9201–9203.
- (21) Abbey, E. R.; Zakharov, L. N.; Liu, S.-Y. *J. Am. Chem. Soc.* **2010**, *132*, 16340–16342.
- (22) Abbey, E. R.; Zakharov, L. N.; Liu, S.-Y. *J. Am. Chem. Soc.* **2011**, *133*, 11508–11511.
- (23) Lemierre, V.; Chrostowska, A.; Dargelos, A.; Chermette, H. *J. Phys. Chem. A* **2005**, *109*, 8348–8355.
- (24) Frisch, M. J.; et al. *Gaussian 09*, revision B.01; Gaussian, Inc.: Wallingford, CT, 2009.
- (25) Raghavachari, K.; Binkley, J. S.; Seeger, R.; Pople, J. A. *J. Chem. Phys.* **1980**, *72*, 650–654.
- (26) (a) Parr, R. G.; Yang, W. *Functional Theory of Atoms and Molecules*; Oxford University Press: New York, 1989. (b) Frisch, M. J.; Trucks, G. W.; Cheeseman, J. R. In *Recent Development and Applications of Modern Density Functional Theory, Theoretical and Computational Chemistry*; Seminario, J. M., Ed.; Elsevier: Amsterdam, 1996; Vol. 4; pp 679–707. (c) Limacher, P. A.; Mikkelsen, K. V.; Lüthi, H. P. *J. Chem. Phys.* **2009**, *130*, 194114. (d) Kobayashi, R.; Amos, R. D. *Chem. Phys. Lett.* **2006**, *420*, 106–109. (e) Jacquemin, D.; Perpète, E. A.; Scalmani, G.; Frisch, M. J.; Kobayashi, R.; Adamo, C. *J. Chem. Phys.* **2007**, *126*, 144105.
- (27) (a) Becke, A. D. *Phys. Rev.* **1988**, *38*, 3098–3100. (b) Becke, A. D. *J. Chem. Phys.* **1993**, *98*, 5648–5652. (c) Lee, C.; Yang, W.; Parr, R. G. *Phys. Rev. B* **1988**, *37*, 785–789. (d) Yanai, T.; Tew, D.; Handy, N. *Chem. Phys. Lett.* **2004**, *393*, 51–57.
- (28) (a) Bartnik, R.; Baylère, P.; Chrostowska, A.; Galindo, A.; Lesniak, S.; Pfister-Guillouzo, G. *Eur. J. Org. Chem.* **2003**, 2475–2479. (b) Chrostowska, A.; Matrane, A.; Maki, D.; Khayar, S.; Ushiki, H.; Graciaa, A.; Belachemi, L.; Guillemin, J.-C. *ChemPhysChem* **2012**, *13*, 226–236. (c) Chrostowska, A.; Dargelos, A.; Khayar, S.; Wentrup, C. *J. Phys. Chem. A* **2012**, *116*, 9315–9320. (d) Vu, T. Y.; Chrostowska, A.; Huynh, T. K. X.; Khayar, S.; Dargelos, A.; Justyna, K.; Pasternak, B.; Leśniak, S.; Wentrup, C. *Chem.–Eur. J.* **2013**, *19*, 14983–14988.
- (29) (a) Stratmann, R. E.; Scuseria, G. E.; Frisch, M. J. *J. Chem. Phys.* **1998**, *109*, 8218–8224. (b) Casida, M. E.; Jamorski, C.; Casida, K. C.; Salahub, D. R. *J. Chem. Phys.* **1998**, *108*, 4439–4449.
- (30) (a) von Niessen, W.; Schirmer, J.; Cederbaum, L. S. *Comput. Phys. Rep.* **1984**, *1*, 57–125. (b) Ortiz, J. V. *J. Chem. Phys.* **1988**, *89*, 6348–6352.
- (31) Nakatsuji, H.; Hirao, K. *J. Chem. Phys.* **1978**, *68*, 2053–2065. See also: <http://www.qcri.or.jp/sacsi/> (accessed June 2014).
- (32) (a) Portmann, S.; Lüthi, H. P. *MOLEKEL 4.3*; Swiss National Supercomputing Center: Lugano, Switzerland. (b) Portmann, S.; Lüthi, H. P. *CHIMIA* **2000**, *54*, 766–770.
- (33) Dolby, L. J.; Hanson, G.; Koenig, T. *J. Org. Chem.* **1976**, *41*, 3537–3539.
- (34) We retook the UV-PE spectrum of natural indole under the same conditions as for its BN isosteres **I** and **II** for direct comparison purposes.
- (35) Chrostowska, A.; Xu, S.; Lamm, A. N.; Mazière, A.; Weber, C. D.; Dargelos, A.; Baylère, P.; Graciaa, A.; Liu, S.-Y. *J. Am. Chem. Soc.* **2012**, *134*, 10279–10285.

(36) Taniguchi, T.; Yamaguchi, S. *Organometallics* **2010**, *29*, 5732–5735.

(37) While many heteroaromatic carbon-boron-nitrogen-containing organic molecules have been synthesized, only a few of them have been experimentally characterized by UV-PES. For examples in addition to reference 35, see: (a) Weber, L.; Domke, I.; Greschner, W.; Miqueu, K.; Chrostowska, A.; Baylère, P. *Organometallics* **2005**, *24*, 5455–5463. (b) ref 19c. (c) Chrostowska, A.; Mazière, A.; Dargelos, A.; Graciaa, A.; Darrigan, C.; Weber, L.; Halama, J. *Eur. J. Inorg. Chem.* **2013**, 5672–5678.

(38) (a) Fukui, K.; Yonezawa, T.; Shingu, H. *J. Chem. Phys.* **1952**, *20*, 722. (b) Fleming, I. *Frontier Orbitals and Organic Chemical Reactions*; Wiley, London, 1978.

(39) A similar phenomenon is also observed for the 1,3-azaborine heterocycle, see: reference 35.

(40) Chen, Z.; Wannere, C. S.; Corminboeuf, C.; Puchta, R.; Schleyer, P. R. *Chem. Rev.* **2005**, *105*, 3842–3888.

(41) For direct comparison purposes, we measured the spectra of these three indoles under identical conditions. See Supporting Information for details.

(42) For direct comparison purposes, we measured the anodic peak potentials of these three indoles under identical conditions. See Supporting Information for details.

(43) For a study of solvent effects on the electrochemical oxidation of substituted anilines, see: Bhuvaneshwari, D. S.; Elango, K. P. *Z. Naturforsch.* **2006**, *61b*, 1254–1260.

(44) Extended exposure of BN indole I to dimethyliminium chloride led to decomposition.

(45) Cheeke, P. R. *Toxicants of Plant Origin: Alkaloids*; CRC press Inc.: Boca Raton, FL, 1989; Vol. 1; pp 172–179.

(46) Greco, M. N.; Hawkins, M. J.; Powell, E. T.; Almond, H. R.; de Garavilla, L.; Hall, J.; Minor, L. K.; Wang, Y.; Corcoran, T. W.; Di Cera, E.; Cantwell, A. M.; Savvides, S. N.; Damiano, B. P.; Maryanoff, B. E. *J. Med. Chem.* **2007**, *50*, 1727–1730.

(47) See Supporting Information for experimental details.

(48) The calculated Mulliken and natural charges are significantly more negative at the C3-carbon than at the C2-carbon, see Supporting Information for details.

(49) The formation of the N-CH<sub>2</sub>-N linkage may be reversible.

(50) The preference for the dimethyliminium chloride to react at the N positions can potentially be explained by the calculated Mulliken and natural charges, which are strongly negative at the nitrogen atoms, see Supporting Information for details.